Design of an Advanced Inlet Liner for the Quiet Technology Demonstrator 3

Douglas M. Nark* and Michael G. Jones†
NASA Langley Research Center, Hampton, VA 23681-2199, U.S.A

The utilization of advanced fan designs (including higher bypass ratios) and shorter engine nacelles has highlighted a need for increased fan noise reduction over a broad frequency range. Thus, improved broadband liner designs must account for these constraints and take advantage of novel liner configurations. With these observations in mind, the development and assessment of a broadband acoustic liner optimization process has been pursued through a series of design and experimental studies. In this work, an advanced inlet liner was designed for a Boeing 737MAX-7 to reduce drag and to improve the broadband noise reduction relative to conventional liners in use today. Specifically, a three layer liner was designed, fabricated, and flight tested as part of the Quiet Technology Demonstrator 3 flight test program. Initial tonal predictions captured the behavior of the measured data very well and both prediction and measurements show an increased acoustic benefit at larger observer angles, particularly at the takeoff condition. Ultimately, flight test results showed the three degree-of-freedom liner to provide a 3.2 EPNdB cumulative inlet component benefit and a 0.7 EPNdB cumulative airplane benefit over the production liner. This excellent result provides valuable validation of the broadband liner design process, as well as the enhancements made to the overall approach. It also illustrates the value of the design process in concurrently evaluating various liner designs (i.e., SDOF, MDOF, etc.) and their application to various locations. Thus, the design process may be applied with further confidence to investigate novel liner configurations in future design studies.

Nomenclature

c	sound speed
h_i	characteristic distance (or height)
i	$\sqrt{-1}$
J_n	Bessel function of order n
k	free-space wave number ($k = \omega/c$)
p	acoustic pressure normalized by ρc^2
T_{ij}	transmission coefficient
u	acoustic particle velocity normalized by c
W_i	weighting values

*Senior Research Scientist, Structural Acoustics Branch, Research Directorate, AIAA Associate Fellow
†Senior Research Scientist, Structural Acoustics Branch, Research Directorate, AIAA Associate Fellow

Symbols:

β	admittance ($\beta = 1/\zeta$)
Γ	propagation constant
ζ	acoustic impedance normalized by ρc ($\zeta = \theta + i\chi$)
θ	acoustic resistance normalized by ρc
θ_o	polar farfield observer angle
μ	mean value
ρ	fluid density
σ	square root of the Prandtl number ($\sigma = \sqrt{Pr}$)
χ	acoustic reactance normalized by ρc
ϕ	azimuthal farfield observer angle
Ω	fraction of treated area
ω	angular frequency

Abbreviations:

CDL	CDUCT-LaRC
GFIT	Grazing Flow Impedance Tube
MDOF	Multidegree of Freedom
SDOF	Single-Degree of Freedom
TRL	Technology Readiness Level
3DOF	Three-Degree of Freedom

I. Introduction

The utilization of advanced fan designs (including higher bypass ratios) and shorter engine nacelles has highlighted a need for increased fan noise reduction over a broad frequency range. Thus, improved broadband liner designs must account for these constraints and take advantage of novel liner configurations.With these observations in mind, the development and assessment of a broadband acoustic liner optimization process has been pursued through a series of design and experimental studies.[1–7] In this design process, an acoustic duct propagation code is used to predict optimum impedance spectra over a number of frequencies and flow conditions. Acoustic liner modeling tools are then used to identify geometric liner parameters (within manufacturing constraints) necessary to produce impedance spectra that most closely match the predicted optimum values. The resultant impedance values are then used with the propagation code to predict attenuation spectra. Iteration between the prediction and design stages is possible to allow refinement of the liner design (e.g., to account for manufacturing constraints).

As the tools used within the broadband liner design process have progressed, a series of multidegree of freedom (MDOF) liner design studies at increasing technology readiness levels (TRL) have been conducted. Initial numerical investigations in the NASA Langley Liner Technology Facility[8,9] (LTF) were positive, as predicted optimum impedance spectra were consistent with those obtained using higher-fidelity, more computationally intensive models. Subsequent design and testing in the NASA Glenn Advanced Noise Control Fan (ANCF) Rig,[3,4] 9-ft x 15-ft Low Speed Wind Tunnel,[5,6] and Aeroacoustic Propulsion Laboratory (AAPL)[7] provided further confidence in the design process. Based on these results and the associated confidence in the modeling and prediction toolchain, an advanced inlet liner was designed for a Boeing 737MAX-7 to reduce drag and to improve the broadband noise reduction relative to conventional liners in use today. The liner was subsequently tested as part of the Quiet Technology Demonstrator 3 (QTD3) flight test program. This paper focuses on the liner design details and performance. The test aircraft and associated measurements are described in Section II. The computational approach, impedance modeling, and liner design process are then presented in more detail in Sections III, IV, and V, respectively. Discussion of the liner performance, as well as initial assessment of prediction accuracy, are provided in Section VI. Finally, concluding remarks regarding some of the more significant results and further areas of interest are presented in Section VII.

II. Test Aircraft and Acoustic Measurements

The QTD3 test article was a Boeing 737 MAX-7 aircraft (see Figure 1) with a modified right hand (starboard side) engine inlet. Acoustic treatment on this engine inlet consisted of either a production inlet liner, the NASA designed inlet liner, or a simulated hard wall configuration (produced by applying speed tape over the inlet acoustic treatment areas). In all cases, the production forward fan case was replaced with a hardwall version. The left hand (port side) engine was a production engine and was flown at idle thrust for all measurements in order to isolate the effects of the inlet liners on the right hand engine. Further discussion of the flight test campaign and data analysis are provided in companion papers.[10,11]

III. Optimum Impedance Prediction

For the current investigation, duct propagation and radiation predictions were conducted using the CDUCT-LaRC (CDL) code. This code calculates the propagation of a given acoustic source ahead of the fan face or aft of the exhaust guide vanes in the inlet or exhaust ducts, respectively. Subsequent to the propagation calculations, the code can compute the noise radiation field outside the duct. The three-dimensional duct modeled using CDL may include acoustic treatment (possibly circumferentially and radially segmented) and incorporate struts/bifurcations. All of the modules that currently make up the CDL framework have been discussed previously[12] and are utilized in this study. However, this discussion will focus on the propagation and radiation modules, as they are most pertinent to this investigation.

The duct propagation module is based on the CDUCT code developed by Dougherty[13,14] and extended by Lan.[15] This code utilizes a parabolic approximation to the convected Helmholtz equation and offers a computationally efficient model that accounts for the complexities of fully three-dimensional nacelle configurations. To provide for such prediction capability, the CDL code supports multiblock propagation calculations in which grid connectivity is determined and data is transferred from upstream to downstream blocks without user intervention.[12] Results of the propagation module include the acoustic potential or pressure within the duct, which may be utilized by the radiation module for acoustic radiation calculations.

The duct radiation model is based on the Ffowcs Williams-Hawkings (FW-H) equation with a permeable data surface.[16] Based on the background flow conditions and propagation solution, this module calculates the radiated acoustic pressure at various observer locations. Currently, the data surface is taken to be the nacelle inlet or exhaust plane for inlet or aft-fan cases, respectively. However, provisions have also been made to attempt to account for the effects of the shear layer on the radiation.

While CDL can accept arbitrary source specification (i.e., it is not a modal code), it is convenient to specify the acoustic source distribution in terms of duct modes. For situations in which the source pressure is available, this greatly simplifies conversion to the required acoustic potential. However, when source information is not available, a source description must be assumed. This is generally the case when considering full or model-scale engines and the approach taken here follows that described by Zlavog and Eversman[17,18] in a series of statistical studies into the effects of randomized modal source power and/or phase on attenuation in lined ducts. In this study, the source modal powers (and hence, amplitudes) and modal phases are allowed to vary randomly and independently. Thus, with equal probability of occurrence, the amplitude and phase for each cut-on source mode may take any value in the intervals from 0 to 1 and 0 to 2π, respectively. This uncertainty in source specification will undoubtedly result in uncertainty in the predicted sound levels. However, as discussed by Zlavog and Eversman,[17,18] transmitted power appears to be normally distributed if the source includes all propagating circumferential and radial acoustic modes with random modal power and phase. In their studies, such a source specification also produced statistical distributions of transmitted power with the smallest standard deviation. Therefore, for each frequency and power setting, 11 source realizations were created to produce a sample population from which statistical information can be inferred. As discussed in a previous CDL study,[19] Student's t-distribution is used to statistically analyze the predicted attenuation results.

As with previous liner optimization studies,[1,3,5] in-duct attenuation was chosen as the cost function for the impedance optimization. Thus, optimum impedance values were predicted using the propagation module of the CDL code (with the aforementioned source model) coupled with optimization routines. This was accomplished by using the Python programming language (http://www.python.org) to "wrapper" the CDL calculations, and allowed access to the full set of tools available in the optimization package of the Scipy[20] library.

IV. Impedance Prediction Model

The impedance prediction model used in this design combines two models presented in an earlier paper.[21] The first is a transmission line model[22] that assumes acoustic wave propagation through each layer of the liner (see Fig. 2), and the second is a lumped element model[23–25] used to compute the impedance change across perforates. The normalized surface impedance spectra presented by each chamber of the liner are computed separately, and are then combined to determine an effective surface impedance spectrum that is assumed uniform across the liner surface.

A. Single Chamber Computations

The transmission line model for predicting the surface acoustic impedance of an individual liner chamber is briefly described herein with the aid of Fig. 2. This figure provides a sketch of a single chamber of a liner with two air gaps (sections with heights of h_1 and h_3) and two perforate sheets (thicknesses of h_2 and h_4). The thickness of each perforate sheet is exaggerated to demonstrate distinct features of the models used in this study. This model treats each unique portion of the liner chamber separately via a transmission line computation. In the following discussion, these unique portions are treated as individual "computational layers."

The transmission line computation is initiated by assuming the backplate at x_0 to be rigid and impermeable. The normalized acoustic pressure and particle velocity are given as

$$\begin{pmatrix} p_0 \\ u_0 \end{pmatrix} = \begin{pmatrix} 1 \\ 0 \end{pmatrix}, \tag{1}$$

which yields an infinite impedance at the backplate of the liner. All acoustic pressures and particle velocities are normalized by ρc^2 and c, respectively, where the density of the air and the speed of sound are for the prevailing static pressure and air temperature. Correspondingly, impedances are normalized by the characteristic impedance of air, ρc. Changes in the acoustic pressure and particle velocity across a computational layer are computed via

$$\begin{pmatrix} p_{n+1} \\ u_{n+1} \end{pmatrix} = \begin{pmatrix} T_{11} & T_{12} \\ T_{21} & T_{22} \end{pmatrix} \begin{pmatrix} p_n \\ u_n \end{pmatrix} \tag{2}$$

where the transmission coefficients (T_{11}, T_{12}, T_{21} and T_{22}) depend on the modeling approach and the type of layer being considered.

For open layers (air gaps), the transmission coefficients are given by

$$T_{11} = T_{22} = cosh(k\Gamma h);\ T_{12} = \zeta_c sinh(k\Gamma h);\ T_{21} = \zeta_c^{-1} sinh(k\Gamma h) \tag{3}$$

where $k = \omega/c$ is the free-space wavenumber, ω is the angular frequency, and h is the layer thickness. The propagation constant, Γ, and characteristic impedance, ζ_c, are computed as

$$\Gamma = \sqrt{\frac{J_0(i^{3/2}s)}{J_2(i^{3/2}s)}}\sqrt{\frac{\gamma}{n_\Gamma}}; \qquad \zeta_c = \frac{-i}{\Gamma}\frac{J_0(i^{3/2}s)}{J_2(i^{3/2}s)} \tag{4}$$

where

$$n_\Gamma = \left[1 + \frac{\gamma - 1}{\gamma}\frac{J_0(i^{3/2}\sigma s)}{J_0(i^{3/2}\sigma s)}\right]^{-1} \tag{5}$$

$i = \sqrt{-1}$ is the imaginary unit, $s = (d_c/2)\sqrt{\rho_s \omega/\mu}$ is the shear wave number, and d_c, ρ_s, ω, μ, σ and γ are the channel diameter, static density, angular frequency, coefficient of viscosity, square root of the Prandtl number and specific heat ratio, respectively. Note that if a liner chamber only contains a single open layer (cavity with no facesheet), the normalized surface impedance for that chamber is computed as

$$\zeta_{ch} = \frac{p_1}{u_1}. \tag{6}$$

For those cases where the liner chamber contains more than one computational layer, the acoustic pressure and particle velocity computed at the top of the first computational layer (p_1 and u_1) are input back into Eq. 2 to compute the impedance change across the next computational layer.

Two approaches are considered for computing the change in impedance across an embedded septum, assumed to consist of either a perforated sheet or a wire mesh. The first assumes the septum to be a purely resistive lumped element that is too thin to support wave propagation. For this approach, the transmission coefficients for Eq. 2 are given by

$$T_{11} = T_{22} = 1; \quad T_{12} = \frac{R_f}{\rho c}; \quad T_{21} = 0 \tag{7}$$

where the normalized DC flow resistance, $R_f/\rho c$, across the perforated sheet is often estimated from a lumped element, semiempirical model.

The second approach assumes the perforated sheet to be sufficiently thick to support wave propagation. Figure 2 is particularly useful to describe this approach. It is assumed that Eqs. 2 and 3 have been used to determine the acoustic pressure and particle velocity (p_{1a} and u_{1a}) at the top of the lower air gap. The acoustic pressure and acoustic mass flow are assumed to be constant across the $\{1a, 1b\}$ interface, such that

$$p_{1b} = p_{1a}; \qquad NS_{1b}u_{1b} = S_{1a}u_{1a}, \tag{8}$$

where N is the number of orifices (3 in this example) connected to a single air cavity, S_{1a} is the cross-sectional area at the top of the air cavity (denoted by the long dashed line at the top of the cavity) and S_{1b} is the cross-sectional area within a single perforate orifice. The wave propagation within the single orifice is then computed using Eqs. 2 and 3, where the orifice diameter is used as the "channel diameter." Again, the acoustic pressure and acoustic mass flow are assumed to be constant across the $\{2a, 2b\}$ interface, such that

$$p_{2b} = p_{2a}; \qquad S_{2b}u_{2b} = NS_{2a}u_{2a} \tag{9}$$

Regardless of which approach is used to model embedded septa (for those configurations that contain them), the process described above is repeated until the acoustic pressure and particle velocity are determined at x_3 (the plane just below the perforated facesheet). The normalized impedance at x_3 is then given by

$$\zeta_{n-1} = \frac{p_{n-1}}{u_{n-1}} \tag{10}$$

($n = 4$ for the example given in Fig. 2). The Two-Parameter Impedance Prediction Model is then used to predict the impedance change across the perforated facesheet, such that the effects of grazing flow over the surface of the liner can be included. The resultant normalized surface impedance for the chamber (at the plane denoted by the dashed line with endpoints *A* and *B*) is given by

$$\zeta_{ch} = \frac{p_n}{u_n} \tag{11}$$

where n represents the number of computational layers in the chamber.

B. Liner Surface Impedance Computation

The surface impedance spectra of the individual chambers are combined to compute the effective impedance across the liner surface. For this computation, it is preferable to use acoustic admittance ($\beta_{ch} = 1/\zeta_{ch}$). The effective admittance across a selected extent of liner surface is given by

$$\beta_s = \Omega \sum_{i=1}^{N_{ch}} \beta_{ch} \tag{12}$$

where N_{ch} represents the number of chambers that combine to form the liner and Ω is the fraction of the surface that is comprised of this group of chambers. The uniform, effective, surface impedance of the liner is then given by $\zeta_s = 1/\beta_s$.

V. Liner Design

As indicated above, the CDL propagation code, coupled with optimization routines, was used to determine optimum impedance values, $\zeta_{opt}(f_i)$, at selected frequencies, f_i, and flight conditions. Specifically, impedance values over a design space encompassing $0 < \theta \leq 5$ and $-10 \leq \chi \leq 10$ were obtained at one-third octave center frequencies ranging from 400 Hz to 10000 Hz at flow conditions representative of approach, cutback, and takeoff flight conditions. The

efficiency of this process allows for a large number of parallel-element, variable-impedance, broadband liner concepts at various technology readiness levels (TRL) to be considered for implementation.

To achieve the desired broadband performance, candidate liner designs consisted of multilayer configurations incorporating septa (or "mesh-caps") embedded into a honeycomb core.[21] This concept allows the acoustic liner to be customized such that the surface impedance of each individual cell is independently controlled. This is achieved by the combination of parameters used to set the impedance in each cell. Clearly, manufacturing constraints (e.g., liner geometric parameters such as porosity and core depth) are key ingredients in this modeling phase, and must be taken into account to design acoustic liners that can be realistically achieved. In this study, the honeycomb cells were allowed to contain up to two mesh-caps. The mesh cap depths and DC flow resistances were allowed to vary from cell to cell. The liner modeling tools were used to obtain design impedance values, $\zeta_{pred}(f_i)$, that minimize the function

$$F = \left\{ \sum_{i=1}^{N} W_i \left(\zeta_{opt}(f_i) - \zeta_{pred}(f_i)\right) \left(\zeta_{opt}(f_i) - \zeta_{pred}(f_i)\right)^* \right\}^{0.5} . \tag{13}$$

Here, the values W_i are weighting factors that may be used to assign increased significance to a selected number of frequencies and/or flow conditions and N is the total number of frequency/flow condition combinations considered. Note that with $W_i = 1$ for all N, equation 13 reduces to the L_2 norm of the difference between the predicted optimum and the design impedance values. As with the first step of the design process, the liner modeling tools were also coupled with the Scipy[20] optimization routines. This replaced the "brute-force" optimization process used previously for this stage of the design process and provided increased efficiency, as well as access to a much wider design space in matching the target impedance spectra.

Based on the above cost function (with the approach, cutback, and takeoff conditions given weighting factors of $W = 0.3$, 0.5, and 1.0, respectively) a number of MDOF liner concepts were considered. As mentioned previously, reduced drag and improved acoustic performance relative to conventional liners were mutual goals of the liner design. Therefore, following previous work related to liner drag reduction, the facesheet employed slots (as opposed to round holes) oriented perpendicular to the flow direction as shown in Figure 3a. Coupled with this facesheet, a 3DOF core (see Figure 3b) was selected that contains two septa in each honeycomb chamber. Each septa has a unique resistance and location within the chamber, and the same distribution is used in each chamber. While a number of candidate MDOF configurations provided good predicted performance, this core configuration was selected based on predicted overall broadband performance and to reduce schedule risk through reduced manufacturing complexity.

A. Build Impedances

The final test article (see Figure 4) incorporating the 3DOF design was the result of the aforementioned design process with adjustments to various liner parameters due to manufacturing constraints. In the liner core, these included a slight reduction in upper septa depth to meet manufacturing tolerances. A reduction in the septa DC flow resistance was also incorporated to reduce schedule risk due to material availability. For the facesheet, the slot widths were increased from 0.02" to 0.031" to allow manufacturing within the test schedule timeframe using production tooling. Further details on the facesheet manufacturing process are provided in a companion paper by Wong.[11]

The impact of these liner parameter modifications on the liner acoustic and drag performance was assessed and deemed acceptable. As part of this process, the liner modeling approach described in Section V was used to predict the impedance of the final 3DOF liner design. Since the model incorporates a conventional perforated facesheet, tests were performed in the NASA Langley Grazing Flow Impedance Tube (GFIT)[26] to estimate the impact of slots versus round holes on the liner impedance. Based on these tests, the predicted (perforate) normalized facesheet resistance was modified according to the following equation

$$\Delta\theta = 0.0002f - 0.0332. \tag{14}$$

The initial perforate and resultant slotted 3DOF impedance spectra are presented in Figure 5. At the time, the mass reactance effects of the slotted facesheet were not considered and therefore, the reactance is unchanged. Based on subsequent observations, this assumption may be reconsidered.

After the flight test, an additional variation in the facesheet parameters was identified. A facesheet thickness of 0.032" was used in the initial modeling. However, with five composite plys and adhesive, the flight test facesheet was actually 0.055" thick. Therefore, additional GFIT testing on 0.032" thick perforate and slotted facesheets, as well as a 0.055" thick slotted facesheet, was undertaken. These facesheets were additively manufactured and placed over a conventional 1.5" deep honeycomb core such that the core reactance could be easily separated from the measurements.

Preliminary results indicated an increase in mass reactance, which may be expected due to the larger mass of air within the slot. However, the measurements also indicated an unexpected effect on resistance. At this time, the results warrant further investigation and additional testing to include a facesheet manufactured in the same manner as the flight test article is planned. Therefore, subsequent in-duct and farfield acoustic predictions presented here employ the impedances based on the initial facesheet (0.032") after modification of the resistance via Eq. 14.

VI. Results and Discussion

Fan noise predictions at one-third octave band center frequencies from 400 Hz to 10000 Hz were carried out to obtain both in-duct and farfield levels. As described in Section III, a statistical source model was employed in which the amplitude and phase of each source mode were randomly selected over a number of trials using a uniform distribution. Note that for a specific engine speed setting, the same random seed was used for each configuration. This provided a consistent source description across the configurations from which acoustic treatment effects could be studied. As discussed by Zlavog and Eversman,[17,18] for the case of all propagating circumferential and radial acoustic modes with random modal power and phase, transmitted power appears to be normally distributed. In their statistical studies, this also produced statistical distributions with the least standard deviation, suggesting the least variable estimate for realized attenuation.

Following this reasoning, the acoustic radiation at the farfield observer locations was taken to be normally distributed. Therefore, Student's t-distribution was used to statistically analyze the predicted results. For each frequency and power setting, 11 simulations were performed to produce a sample population from which statistical information could be inferred. Following the discussion in Coleman and Steele,[27] the sample mean, $\bar{X}$, is computed as

$$\bar{X} = \frac{1}{N}\sum_{i=1}^{N} X_i$$

where N is the number (11 in this case) of individual samples X_i. The sample standard deviation, S_X, is defined by

$$S_X = \left[\frac{1}{N-1}\sum_{i=1}^{N}\left(X_i - \bar{X}\right)^2\right]^{1/2}$$

and the sample standard deviation of the mean, $S_{\bar{X}}$, is given by

$$S_{\bar{X}} = \frac{S_X}{\sqrt{N}}.$$

Thus, the 95% confidence limit for a sample of N measurements of X taken from a Gaussian distribution may be defined as the random uncertainty, P, where

$$P_{\bar{X}} = tS_{\bar{X}} = \frac{tS_X}{\sqrt{N}}$$

and t is determined by the t-distribution ($t = 2.23$ for this case with $N = 11$ and 95% probability). Considering sample populations drawn from a Gaussian parent distribution, the $\pm P$ interval provides the interval within which the population mean, μ, is expected to lie with 95% confidence. The expression for this 95% confidence interval may be written

$$\text{Prob}\left(\bar{X} - P_{\bar{X}} \leq \mu \leq \bar{X} + P_{\bar{X}}\right) = 0.95.$$

Thus, in addition to providing source information when specific modal source content is not available, this approach provides confidence intervals to aid in acoustic treatment assessment.

As mentioned above, in-duct attenuation was chosen as the cost function for the impedance optimization. Results for the 3DOF liner at the three flight conditions are presented in Figure 6. Errors bars are also included to represent the 95% confidence intervals on the predicted values. The overall predicted in-duct attenuation increases with increased flow speed progressively from approach to the takeoff condition. At each condition, the attenuation is maximum at the lower frequencies, is reduced for the middle frequencies, and then may have a slight increase (remaining below the maximum) at the higher frequencies. The 95% confidence intervals also decrease as the frequency increases, which may partly be due to the increase in source modal content.

Farfield acoustic predictions were also obtained on a hemisphere (150 feet radius) centered on the engine inlet using the CDL radiation module described in Section III. Observer locations extend from polar angles, θ_o, of 5° to

90° from the inlet in 5° increments as shown in Figure 7. Radiation angles greater than 90° were not included in the predictions due to the nature of the FW-H source surface. Four distinct observer arcs separated azimuthally by 90° are also indicated by thick red lines in this figure. As seen in Figure 8, these locations are used to illustrate the variation in directivity due to the asymmetric nature of the inlet geometry. Here, the mean sound pressure level (SPL) for the 3DOF liner configuration at a one-third octave band center frequency near the blade passage frequency (for the given flight condition) is shown for each observer arc. There are variations over the full set of flight conditions, with a larger deviation in the peak directivity angle for the takeoff condition. These variations may fall within the 95% confidence intervals in many instances. However, the asymmetric nature of the radiated field is clearly evident and may need to be considered when making comparisons with measurements (or other predictions).

In Figure 9, mean sound pressure levels for the 3DOF and hardwall configurations at a one-third octave band center frequency near the blade passage frequency (for the given flight condition) are presented along the bottom of the hemisphere ($\phi = 180°$). The 95% confidence intervals are again represented by error bars and show the variability that may be encountered when dealing with tone predictions. It should be noted that the statistical analysis was performed on a p^2 basis and resulted in single values for the upper/lower bounds of the 95% confidence interval related to this quantity. However, the conversion to decibel levels leads to larger confidence intervals on the lower bounds due to the logarithmic nature of the calculation. Since the results are based on 11 simulations, this can result in fairly large lower bounds on the 95% confidence intervals (for example, the 50° observer location for the takeoff condition). However, the general behavior may be inferred from the mean values and these bounds could likely be reduced by increasing the number of simulations considered. Considering the mean SPL levels, the 3DOF liner provides a clear acoustic benefit for observer angles above 50°. When the 95% confidence intervals are also considered, the 3DOF liner appears to provide a slight benefit at the lower observer angles as well. Overall, the predictions suggest an increased acoustic benefit for the 3DOF liner with increasing flight speed, which is consistent with the in-duct predictions. Future work includes plans for additional post-test predictions. However, further investigation into the impact of the facesheet parameters discussed previously will be pursued prior to presenting comparisons with measured data.

The QTD3 acoustic flyover testing was conducted at the Grant County International Airport in Moses Lake, WA in the summer of 2018. The results of the test data analysis were described by Wong,[11] including measured tonal levels the blade passage frequency for the cutback and takeoff conditions. The predictions described above match the measured results very well and both show an increased benefit at larger observer angles that increases at the takeoff condition. Overall, the flight test results show that the 3DOF liner achieved a component and aircraft level acoustic benefit over all three certification flight conditions. Specifically, measurements indicated that the 3DOF design provided effective broadband noise reduction at the approach condition and significant tonal noise reduction at the takeoff condition. Ultimately, the 3DOF liner provided a 3.2 EPNdB cumulative inlet component benefit and a 0.7 EPNdB cumulative airplane benefit over the production liner.

VII. Concluding Remarks

This paper describes the extension of a broadband acoustic liner design process to the inlet of the QTD3 flight test aircraft. Based on in-duct attenuation predictions and liner modeling tools, a 3DOF liner was designed, fabricated, and flight tested. Initial tonal predictions captured the behavior of the measured data very well and both show an increased benefit at larger observer angles, particularly at the takeoff condition. Future work will include further investigation of the impacts of perforated versus slotted holes for facesheets of various thickness. Subsequently, further comparison between tonal and broadband predictions and measurements will be performed.

Ultimately, flight test results showed the 3DOF liner to provide a 3.2 EPNdB cumulative inlet component benefit and a 0.7 EPNdB cumulative airplane benefit over the production liner. This excellent result provides valuable validation of the broadband liner design process, as well as the enhancements made to the overall approach. It also illustrates the value of the design process in concurrently evaluating various liner designs (i.e., SDOF, MDOF, etc.) and their application to various locations. Thus, the design process may be utilized with increased confidence to investigate novel liner configurations in future design studies.

Acknowledgments

This research was funded by the Advanced Air Transport Technology (AATT) Project of the NASA Advanced Air Vehicles Program (AAVP). The authors would like to acknowledge Andres Baca and Clark Smith of the Hexcel Corporation for their expertise in the liner core manufacturing. Hamilton Fernandez from NASA Langley and Eric Nesbitt, Belur Shivashankara, and Jackie Wong from the Boeing Corporation were also instrumental in the development of the

QTD3 test flight campaign.

References

[1]Nark, D. M. and Jones, M. G., "Broadband Liner Optimization for the Source Diagnostic Test Fan," AIAA Paper 2012-2195, 2012.

[2]Nark, D. M., Jones, M. G., Sutliff, D. L., Ayle, E., and Ichihashi, F., "Improved Broadband Liner Optimization Applied to the Advanced Noise Control Fan," AIAA Paper 2014-3103, 2014.

[3]Nark, D. M., Jones, M. G., and Sutliff, D. L., "Modeling of Broadband Liners Applied to the Advanced Noise Control Fan," AIAA Paper 2015-2693, 2015.

[4]Sutliff, D. L., Jones, M. G., and Nark, D. M., "In-Duct and Far-field Experimental Measurements from the ANCF for the Purpose of Improved Broadband Liner Optimization," AIAA Paper 2014-3231, 2014.

[5]Nark, D. M., Jones, M. G., and Sutliff, D. L., "Further Development and Assessment of a Broadband Liner Optimization Process," AIAA Paper 2016-2784, 2016.

[6]Sutliff, D. L., Nark, D. M., and Jones, M. G., "Efficacy of a Multiple Degree of Freedom Acoustic Liner Installed in the Bypass of a Scale Model High Speed Fan," AIAA Paper 2016-3005, 2016.

[7]Nark, D. M., Jones, M. G., Schiller, N. H., and Sutliff, D. L., "Broadband Inlet Liner Design for the DGEN Aeropropulsion Research Turbofan," AIAA Paper 2018-3608, 2018.

[8]Gerhold, C. H., Brown, M. C., and Jones, M. G., "Segmented Liner to Control Mode Scattering," AIAA Paper 2013-2078, 2013.

[9]Jones, M. G., Watson, W. R., and June, J. C., "Optimization of Microphone Locations for Acoustic Liner Impedance Eduction," AIAA Paper 2015-3271, 2015.

[10]Brusniak, L., Wong, J., Jones, M., and Nark, D., "Acoustic Phased Array Analysis of Quiet Technology Demonstrator 3 Advanced Inlet Liner Noise Components," AIAA Paper 2019-xxxx, 2019.

[11]Wong, J., Nesbitt, E., Jones, M., and Nark, D., "Flight Test Methodology for NASA Advanced Inlet Liner on 737MAX-7 Test Bed (Quiet Technology Demonstrator 3)," AIAA Paper 2019-xxxx, 2019.

[12]Nark, D. M., Farassat, F., Pope, D. S., and Vatsa, V., "The Development of the Ducted Fan Noise Propagation and Radiation Code CDUCT-LaRC," AIAA Paper 2003-3242, 2003.

[13]Dougherty, R. P., "A Wave-Splitting Technique for Nacelle Acoustic Propagation," AIAA Paper 97-1652, 1997.

[14]Dougherty, R. P., "A Parabolic Approximation for Flow Effects on Sound Propagation in Nonuniform, Softwall, Ducts," AIAA Paper 99-1822, 1999.

[15]Lan, J. H., "Turbofan Duct Propagation Model," NASA CR 2001-211245, 2001.

[16]Brentner, K. B. and Farassat, F., "Analytical Comparison of the Acoustic Analogy and Kirchhoff Formulation for Moving Surfaces," *AIAA Journal*, Vol. 36, No. 8, 1998, pp. 1379–1386.

[17]Zlavog, G. and Eversman, W., "Source effects on attenuation in lined ducts. Part I: A statistically based computational approach," *Journal of Sound and Vibration*, Vol. 307, No. 1-2, 2007, pp. 113–138.

[18]Zlavog, G. and Eversman, W., "Source effects on attenuation in lined ducts. Part II: Statistical properties," *Journal of Sound and Vibration*, Vol. 307, No. 1-2, 2007, pp. 139–151.

[19]Nark, D. M., "Assessment of Radiated Fan Noise Prediction Capabilities using Static Engine Test Data," AIAA Paper 2011-2807, 2011.

[20]Jones, E., Oliphant, T., Peterson, P., et al., "SciPy: Open source scientific tools for Python," 2001 -.

[21]Jones, M. G., Howerton, B. M., and Ayle, E., "Evaluation of Parallel-Element, Variable-Impedance, Broadband Acoustic Liner Concepts," AIAA Paper 2012-2194, 2012.

[22]Parrott, T. L. and Jones, M. G., "Parallel-Element Liner Impedances for Improved Absorption of Broadband Sound in Ducts," *Noise Control Engineering Journal*, Vol. 43, No. 6, 1995, pp. 183–195.

[23]Motsinger, R. E. and Kraft, R. E., "Design and Performance of Duct Acoustic Treatment: Aeroacoustics of Flight Vehicles; Chapter 14, Vol. 2: Noise Control," NASA RP 1258, August 1991.

[24]Jones, M. G., Parrott, T. L., and Watson, W. R., "Uncertainty and Sensitivity Analyses of a Two-Parameter Impedance Prediction Model," AIAA Paper 2008-2928, 2008.

[25]Parrott, T. L. and Jones, M. G., "Assessment of NASA's Aircraft Noise Prediction Capability, Chapter 6: Uncertainty in Acoustic Liner Impedance Measurement and Prediction," NASA TP 2102-215653, July 2012.

[26]Jones, M. G., Watson, W. R., Parrott, T. L., and Smith, C. D., "Design and Evaluation of Modifications to the NASA Langley Flow Impedance Tube," AIAA Paper 2004-2837, 2004.

[27]Coleman, H. W. and Steele, W. G., *Experimentation and Uncertainty Analysis for Engineers*, John Wiley & Sons, Inc., 1999.

Figure 1: Boeing 737MAX-7 (Quiet Demonstrator 3) Test Aircraft.

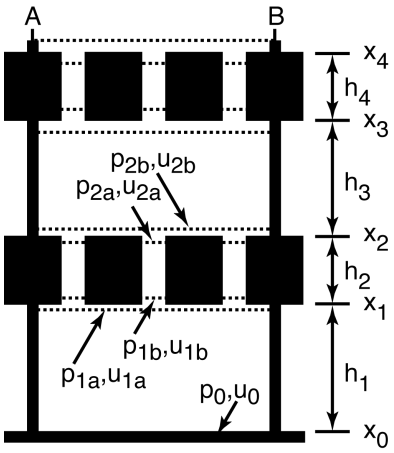

Figure 2: Sketch of single chamber of a liner with key parameters for transmission line impedance prediction model.

(a) Facesheet sample illustrating perpendicular flow slots.

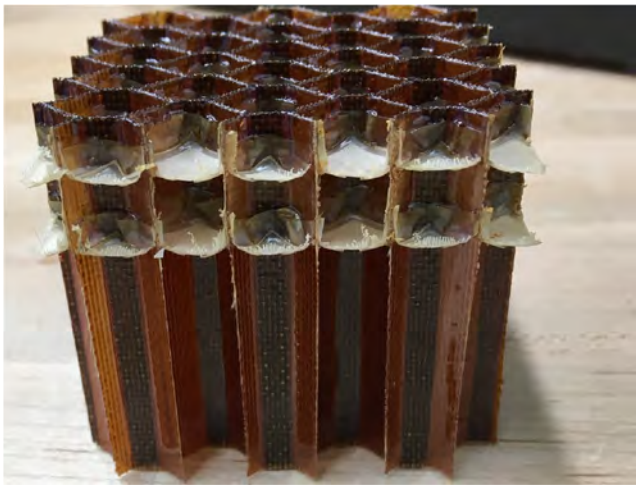

(b) 3DOF liner core.

Figure 3: Inlet liner components.

Figure 4: QTD3 flight inlet.

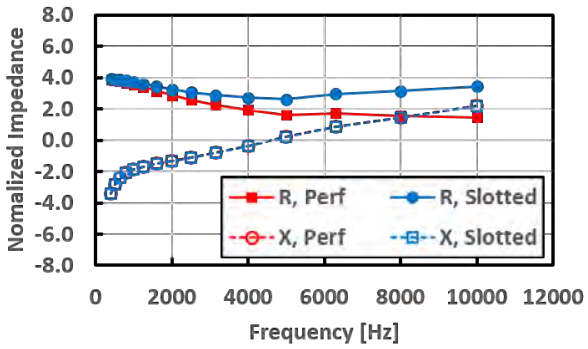

(a) Approach

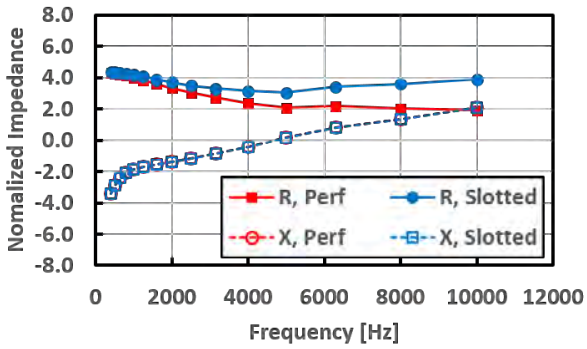

(b) Cutback

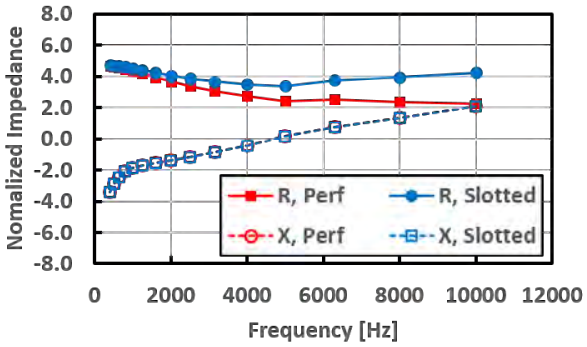

(c) Takeoff

Figure 5: Predicted 3DOF impedance spectra at the three flight conditions considered.

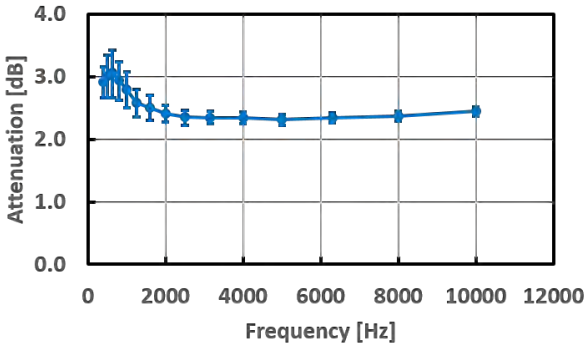

(a) Approach

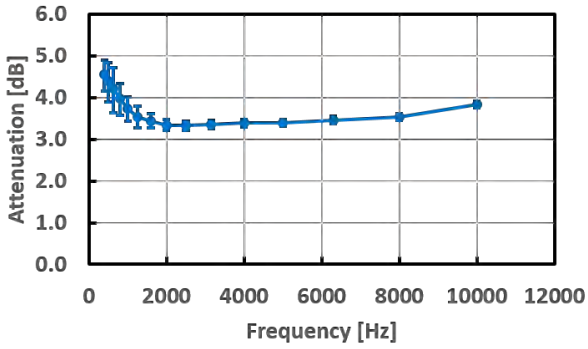

(b) Cutback

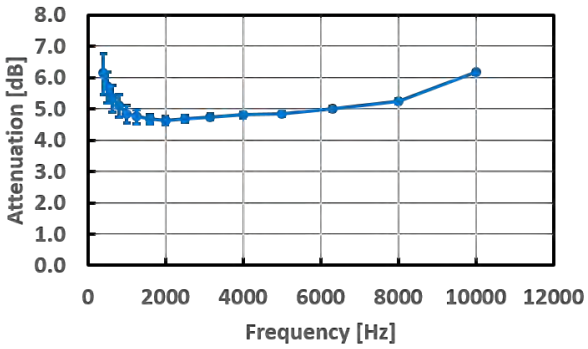

(c) Takeoff

Figure 6: Predicted in-duct attenuation at the three flight conditions considered.

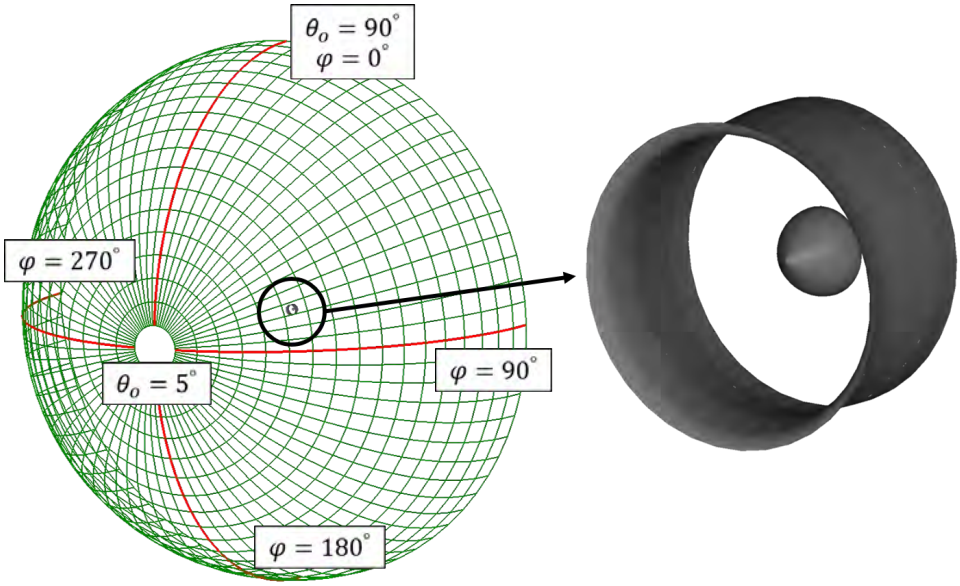

Figure 7: Observer hemisphere (radius, $r = 150$ ft.) centered on the engine axis.

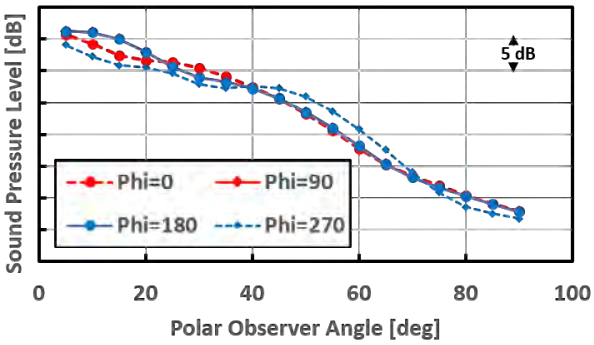

(a) Approach

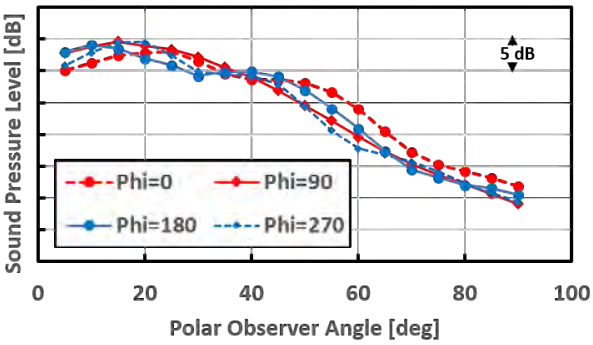

(b) Cutback

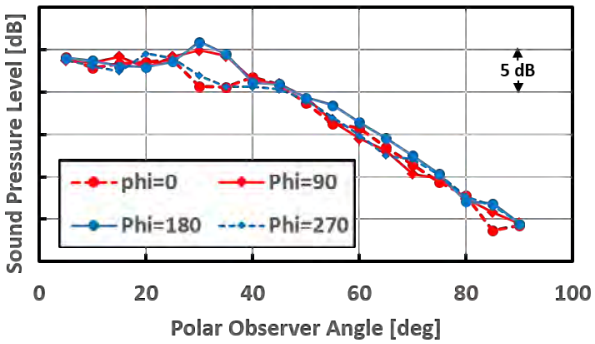

(c) Takeoff

Figure 8: Predicted mean tonal sound pressure level (SPL) at four azimuthal angles. The tones are one-third octave band center frequencies nearest the blade passage frequency for each flight condition.

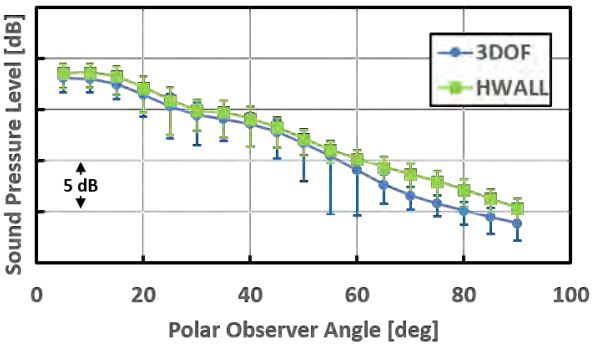

(a) Approach

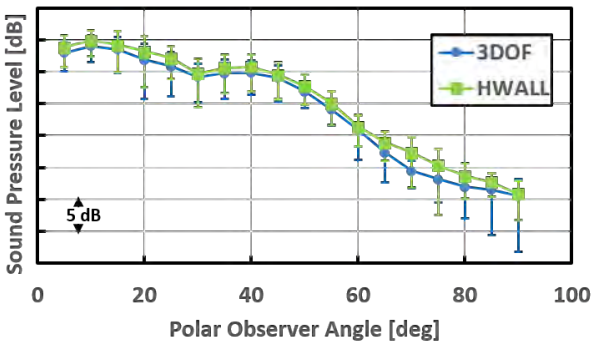

(b) Cutback

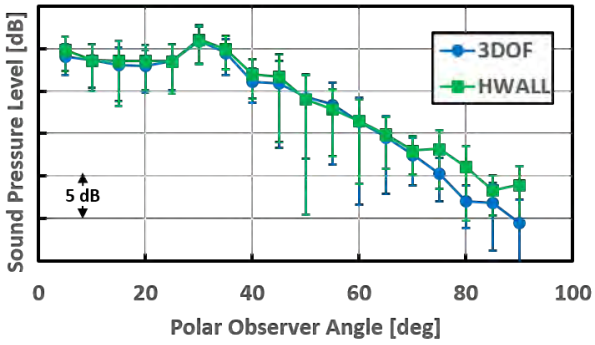

(c) Takeoff

Figure 9: Predicted mean tonal sound pressure level (SPL) for observers on the bottom of the farfield hemisphere ($\phi = 0^\circ$). The tones are one-third octave band center frequencies nearest the blade passage frequency for each flight condition. Error bars represent 95% confidence intervals on the predicted SPL values.